

## Galvanic Corrosion of the Base AISI 316L/Micro-Plasma Arc Welded AISI 316L in Polluted Phosphoric Acid Media at Different Temperatures

R. Sánchez-Tovar<sup>1</sup>, M.T. Montañés<sup>1</sup>, J. García-Antón<sup>1,\*</sup>, A. Guenbour<sup>2</sup>

<sup>1</sup> Ingeniería Electroquímica y Corrosión (IEC), Departamento de Ingeniería Química y Nuclear. E.T.S.I. Industriales, Universitat Politècnica de València, 46022 Valencia. Spain

Phone: +34 963877632 Fax: +34 963877639

<sup>2</sup> Laboratoire de Corrosion-Electrochimie. Faculté des Sciences, Université Mohammed V- Agdal, BP 1014 Rabat. Morocco.

\*E-mail: [jgarciaa@iqn.upv.es](mailto:jgarciaa@iqn.upv.es)

Received: 17 June 2011 / Accepted: 13 July 2011 / Published: 1 August 2011

---

In this work, the galvanic corrosion of the base AISI 316L stainless steel/micro-plasma arc welded AISI 316L stainless steel in phosphoric acid solutions polluted with sulphuric acid and chlorides was studied by means of the Zero-Resistance Ammeter technique. Experiments were performed at different temperatures (25, 40 and 60 °C) under flowing conditions (Reynolds number of 1456). Galvanic current density values are negative during the first hour of the test indicating that the welded alloy is corroding; then, they shift towards positive values indicating that the base stainless steel corrodes. Galvanic current density values reached stable values from the third hour of the tests performed at 25 and 40 °C, and during the last two hours of the test at 60 °C indicating passivation of the base alloy. Uniform corrosion processes occur for the AISI 316L alloy in polluted phosphoric acid solutions. Galvanic current densities increase with temperature according to Arrhenius plot. Impurities seem to increase galvanic corrosion and hinder passivation processes.

---

**Keywords:** Phosphoric acid; AISI 316L stainless steel; Galvanic corrosion; Welding; Zero-resistance ammeter.

### 1. INTRODUCTION

The wet acid process is widely used for the phosphoric acid production. The process consists of the attack of the phosphate ore with sulphuric acid; then, the phosphoric acid is filtered to separate calcium sulphates and following, it is concentrated to the desired grade. Several impurities appear in this process such as chlorides, fluorides, sulphates, SiO<sub>2</sub>, Al<sup>+3</sup>, Mg<sup>+2</sup>, Ca<sup>+2</sup>, Fe<sup>+3</sup> and so on, depending on the phosphate rock.

In particular, the rests of sulphuric acid (which is used in excess) and the presence of chlorides increase corrosion processes in the metallic elements of industrial phosphoric acid plants. Extremely severe corrosive conditions occur in the reaction tanks, especially corrosion-erosion of the agitators. In fact, fluid flow has been considered to enhance the corrosion problems [1, 2]. Moreover, in the evaporators the heat exchanger metal walls reached high temperatures. Additionally, significant corrosion problems can also take place during transportation, handling and storage operations [3].

Austenitic stainless steels (SS) have good corrosion resistance to chemically pure phosphoric acid over a wide range of concentrations and temperatures [4-6]. Particularly, AISI 316L stainless steels are commonly used due to their combined corrosion resistance and good mechanical properties [7].

Furthermore, austenitic stainless steel is among the easiest alloys to weld which allows the fabrication of very tough welded joints even under as-welded conditions, without any further treatment [8]. However, welding processes cause residual stresses and metallurgical changes [9-13] increasing the dissimilarity of the base metal-weld metal pair and causing galvanic corrosion [14]. AISI 316L SS tend to undergo pitting corrosion, especially in media with chloride ions [15]. Galvanic corrosion is one of the most common and damaging forms of corrosion. Hence, controlling galvanic corrosion is of great economic importance in many industries [16].

Nowadays, the use of the Zero-Resistance Ammeter (ZRA) electrochemical technique is gaining importance, since it can be used without disturbing the system under study and in continuous-time [17].

ZRA consists of the register of the naturally occurring fluctuations in the potential and current of corroding electrodes that take place during a corrosion process [18]. The evaluation of the ZRA measurements can be used to determine the corrosion mechanism and the corrosion rate [19].

Some works have studied the corrosion behaviour of stainless steels in polluted phosphoric acid [20-23] and the effect of temperature on the corrosion resistance of the materials. However, none of these studies was performed under flowing conditions, which are the real operating conditions in the industrial sector.

Similarly, very few works have analysed the influence of flow rate on the corrosion behaviour of stainless steels in polluted phosphoric acid media [24] using potentiodynamic polarization curves; however, galvanic corrosion resulting from the presence of another metal or alloy has not been studied. The purpose of this work is to study the galvanic corrosion behaviour of the base AISI 316L/welded AISI 316L pair in phosphoric acid solutions polluted by sulphuric acid and chlorides working under hydrodynamic conditions (using a Reynolds number (Re) of 1456). The micro-plasma arc welding (MPAW) technique will be used for the welds; MPAW is a variation of the plasma arc welding process that uses intensities lower than 20 A and allows for greater energy concentration, deeper and narrower penetration and greater arc stability.

The corrosion evaluation was carried out by means of Zero-Resistance Ammeter electrochemical measurements. The effect of temperature was also taken into consideration (25, 40 and 60 °C). The tests were further compared to those obtained in pure phosphoric acid solutions.

## 2. MATERIALS AND METHODS

### 2.1. Materials

The AISI 316L stainless steels used in this work were tubes 14 mm and 16 mm in inner and external diameter, respectively, and 20 mm in length, having an area of 8.8 cm<sup>2</sup> exposed to the solution. The base material was AISI 316L SS and it was welded with AISI 316L filler alloy and with argon backing gas (99.9%); their composition is shown in Table 1.

**Table 1.** Composition of AISI 316L base material and filler alloy given by the manufacturer (% wt.).

AISI 316L	Cr	Ni	Mn	Mo	S	Si	P	C	Fe
Base	16.957	10.171	1.337	2.298	0.004	0.368	0.030	0.022	Bal.
* Filler alloy	18.160	12.100	1.860	2.540	0.007	0.760	0.018	0.010	Bal.
* Filler alloy also contains Cu: 0.080% wt. and N: 0.050% wt.									

#### 2.1.1. Welding technique

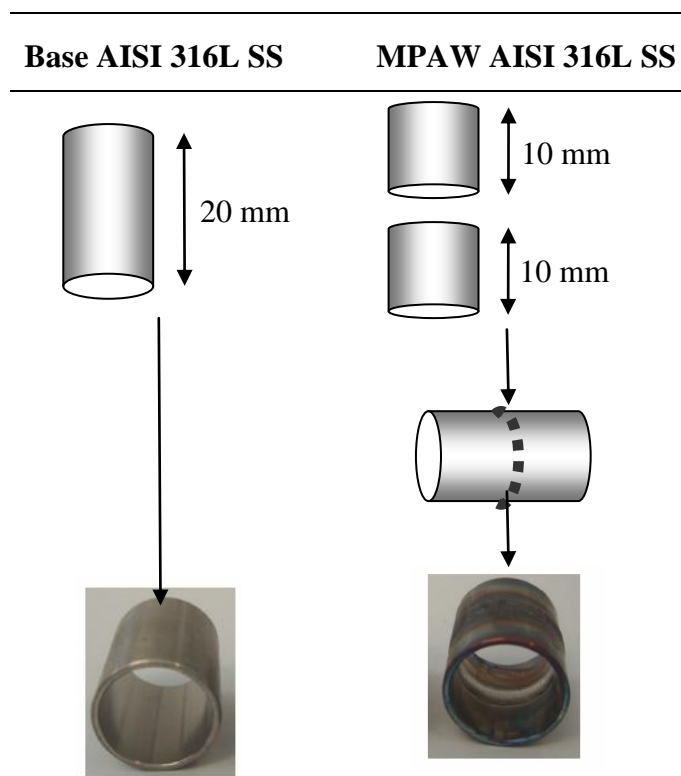


**Figure 1.** Scheme and photographs of the tubes: base and MPAW AISI 316L SS.

Micro-plasma arc welding was performed on two tubes 10 mm in length. The argon backing gas was used to protect the inner surface of the materials during welding [25]. The flow rate of this

shielding gas was 2.5 L/min. The welding process was carried out in two steps (step one: current = 11.3 A, voltage = 20 V, welding speed = 2.6 mm/s, and step two: current = 13 A, voltage = 20 V, welding speed = 2.6 mm/s). The flow rate of the plasma gas was 6.5 L/min. Figure 1 shows a photograph of the non-welded and the micro-plasma arc welded AISI 316L SS tubes.

### 2.1.2. Microstructure evaluation

In order to evaluate the microstructural variations resulting from the micro-plasma arc welding, the tubes were cut lengthwise and covered in cold mounting acrylic resin (DuroFix-2, Struers) for the embedding of specimens. Then, the samples were wet abraded from 220 silicon carbide (SiC) grit to 4000 SiC grit (in several steps; i.e. 220, 500, 1000, 2500 and 4000). The mounted samples were polished with 1 and 0.3 micron alumina and were rinsed with distilled water, followed by ethanol and air-dried. Once the samples were polished, they were etched by modified Kiesel metallographic etching according to ASM International [26]. The etchant composition consisted of 10 mL of nitric acid (65 wt. %), 10 mL of acetic acid (99-100 wt. %), 15 mL of hydrochloric acid (37-38 wt. %) and 5 mL of glycerine (100 wt. %). The samples were immersed in the etching solution during 90 seconds and then rinsed with distilled water, followed by ethanol and air-dried. Subsequently, materials were examined by light microscopy (LM) and their microstructure was compared to that of the base alloy.

## 2.2. Operating conditions

### 2.2.1. Hydrodynamic circuit

A hydrodynamic circuit, described elsewhere [27], was used to study galvanic corrosion. The circuit consisted of a centrifugal pump, a flow-meter, a thermostat to regulate the solution temperature, a test section (where the tubes are assessed), a valve to drain the system and several glass devices: for the reference electrode (Ag/AgCl, 3M KCl), for a thermometer to control the temperature, for the gas output, a device to introduce the solution into the flow circuit and another device to bubble an inert gas. Medical grade silicone flexible tubes were used to assemble the different elements. Fully developed flow was assured using a 90-cm-long Teflon rigid tube of the same inner diameter as the test tubes upstream of the test section.

### 2.2.2. Concentration and temperature

Materials were tested in a  $\text{H}_3\text{PO}_4$  solution 40 wt. % (5.5 M) polluted with sulphuric acid 2% wt. (0.26 M) and chlorides 0.03% wt. (380 ppm), prepared from KCl. The experiments were carried out at a Reynolds number of 1456 at 25, 40 and 60 °C; that is at the flow rates of 171, 121 and 82 L/h of polluted phosphoric acid solution for each temperature, respectively. These concentration and temperature conditions are typical in the phosphoric acid industry [28].

### 2.3. Electrochemical tests

Zero-Resistance Ammeter measurements were used to study galvanic corrosion. A potentiostat (Solartron 1285 provided with the Corrware software) was used to perform the tests. Before each test, the tubes were rinsed with distilled water, degreased with ethanol and dried with air at room temperature. Nitrogen (99.99 %) was bubbled for 60 minutes prior to the tests. All the tests were repeated at least three times in order to verify reproducibility.

The galvanic current density ( $i_G$ ) and galvanic potential ( $E_G$ ) between the pair were measured with ZRA every 0.5 s for 8 h. The tests were designed with the base AISI 316L SS as working electrode (WE) and the micro-plasma arc welded AISI 316L SS grounded. Figure 2 shows a diagram of the physical configuration of the electrodes in the test section. The tubes were insulated with a Teflon intermediate assembly piece 14 mm in inner diameter, as well as the inner diameter of the tubes. Current sign was positive when the electrons flowed from the base alloy (working electrode) to the potentiostat; indicating that base AISI 316L SS was corroding. However, current values were negative when the electrons flowed in the opposite direction, that is, the micro-plasma arc welded AISI 316L SS was corroding.

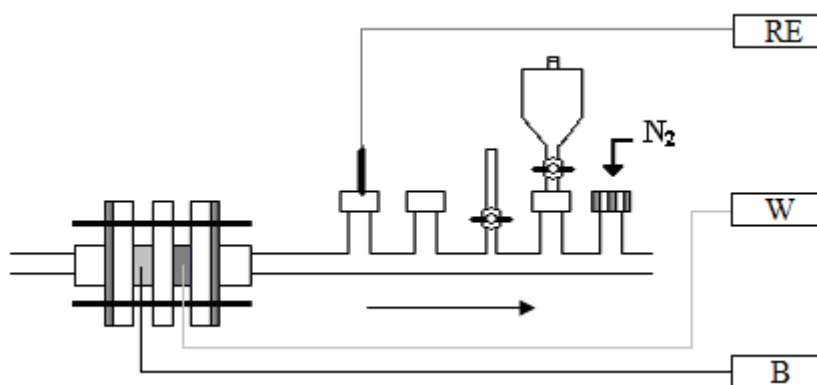


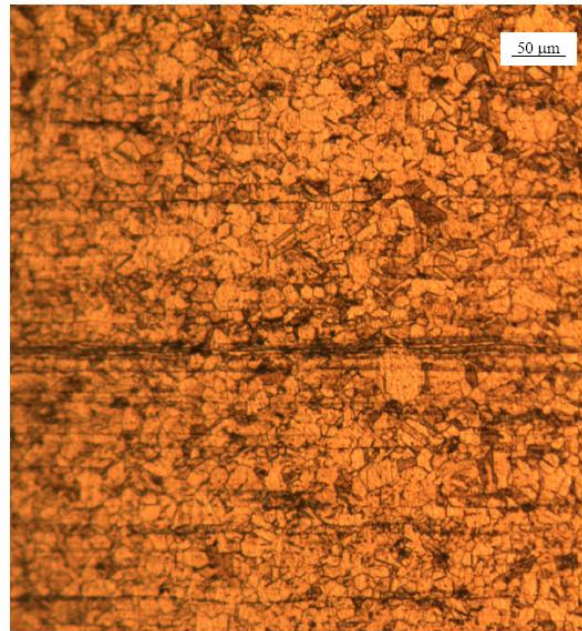
**Figure 2.** Diagram of the configuration of the electrodes in the test section. RE: reference electrode, B: base AISI 316L SS and W: micro-plasma arc welded AISI 316L SS.

## 3. RESULTS AND DISCUSSION

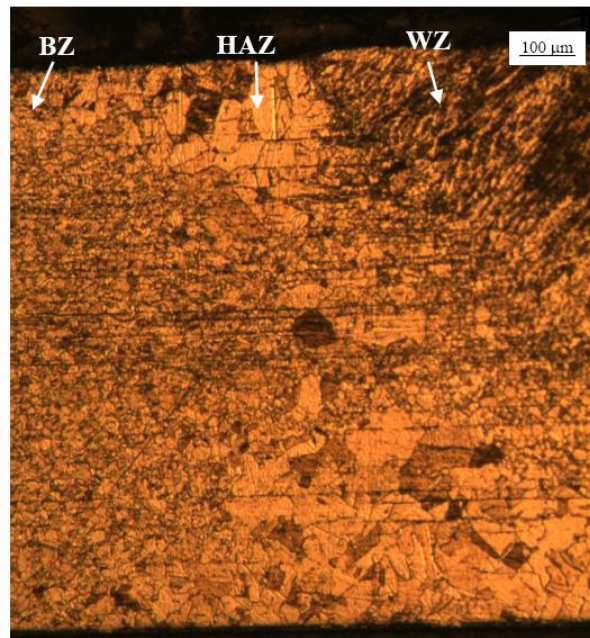
### 3.1. Materials analysis

As mentioned in the materials and methods section, the tubes were cut lengthwise, covered in resin and etched in order to evaluate their microstructure. The effect of the micro-plasma arc welding procedure on the AISI 316L SS microstructure was also taken into account, by comparing the base and the welded stainless steel microstructures. Light microscopy was used to observe the microstructure of the materials. Figure 3 shows the microstructure of the base AISI 316L SS (Figure 3a) and the MPA welded AISI 316L SS (Figure 3b) after etching.

Figure 3a shows that the microstructure of the base AISI 316L SS is characterised by an austenitic single-phase with equiaxed grains, where twins can also be observed.



A) Base AISI 316L SS



B) MPA welded AISI 316L SS

**Figure 3.** Microstructure of the AISI 316L SS acquired by LM. a. Base AISI 316L SS and b. Micro-plasma arc welded AISI 316L SS.

Figure 3b shows that the microstructure of the welded AISI 316L is different from that of the base material. This indicates that the micro-plasma arc welding process introduces microstructural

changes in AISI 316L SS. In Figure 3b, three different zones can be distinguished in terms of grain shape. The weld zone (weld bead) possesses columnar grains where delta-ferrite can be found [26]. Alloys with especially low carbon contents, such as AISI 316L SS, present a greater tendency towards delta-ferrite stabilization, in order to minimize susceptibility to sensitization during welding [26]. Delta-ferrite presents two opposite phenomena: on the one hand, it increases the resistance to hot cracking [29, 30] but, on the other hand, it also reduces corrosion resistance due to the formation of a less stable passive film [31]. The zone close to the weld zone was named heat affected zone (HAZ); HAZ has a single austenitic microstructure with equiaxed grains, but it is characterised by an increase in grain size [32]. The zone farther from the weld zone has a single austenitic microstructure with grain size very similar to that observed in the base AISI 316L SS, for this reason it will be called base zone. It can be pointed out that in both Figures, 3a and 3b carbide precipitation was not observed since AISI 316L SS is a stainless steel with low carbon content.

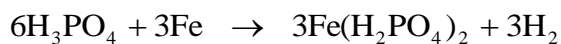
## 3.2. Galvanic corrosion

### 3.2.1. Galvanic current density and galvanic potential profiles in polluted $H_3PO_4$ media.

As it has been proved, micro-plasma arc welding introduces changes in the AISI 316L SS microstructure; these changes generate dissimilarities between the base and welded stainless steel, which could result in the formation of a galvanic pair when the tubes are in electrical contact with polluted phosphoric acid solutions. In order to analyse the possible galvanic corrosion of the base AISI 316L SS/MPA welded AISI 316L SS pair, ZRA tests were performed.

Figure 4 shows the galvanic current density ( $i_G$ ) and the galvanic potential ( $E_G$ ) profiles of the base AISI 316L SS/MPA welded AISI 316L SS pair in polluted  $H_3PO_4$  at a Re of 1456 and at different temperatures: 25, 40 and 60 °C. Since the tests were reproducible, Figure 4 shows only one of the profiles obtained after 8 hours.

Figure 4 shows that galvanic current densities are negative during the first hour of the tests at all the temperatures studied. Therefore, during this first hour, the anode of the pair is the micro-plasma arc welded AISI 316L SS. Moreover, during the first minutes of the test working at 60 °C, the galvanic current density profile undergoes an abrupt shift through positive values, followed by a trend towards negative ones. This sharp shift is attributed to the initial contact of the materials with the solution. On the other hand, the general tendency of the galvanic current density during the first hour is to decrease with time (in absolute value). This trend is more noticeable as temperature increases. Consequently, from the second hour to the end of the tests, the galvanic current densities registered are always positive. That is, during the first hour of the test, micro-plasma arc welded material passivation takes place and there is a change in polarity indicating that the base AISI 316L SS is corroding. Concretely chromium oxide is considered the main passive component of the passive film in the anodic polarization of stainless steels. On the other hand, phosphoric acid media favour the formation of iron phosphates [33]. Phosphate species can precipitate with dissolved iron species to form iron phosphates, since these compounds are characterised by a low solubility. Precipitation of iron phosphate occurs at the interface [34]; that is:



In phosphoric acid solutions, the passivation process is a combination of an inner chromium oxide layer together with an outer one formed with soluble  $\text{Fe}(\text{H}_2\text{PO}_4)_2$  and the insoluble compounds  $\text{FeHPO}_4$  and  $\text{Fe}_3(\text{PO}_4)_2$  [35].

At the lower temperatures studied (25 and 40 °C), galvanic current density stabilised after the third hour of the test; probably due to the formation of a passive layer on the base AISI 316L SS [36]. However, at 60 °C, stabilisation occurred after the seventh hour. It could be concluded that temperature prevents the passivation of the base AISI 316L SS.

Once the system is stabilised (from the third hour of the tests performed at 25 and 40 °C, and after the seventh hour of the test at 60 °C), the lowest galvanic current density values were obtained at 25 °C (around 4  $\mu\text{A}/\text{cm}^2$ ), at 40 °C  $i_G$  stabilises at around 5  $\mu\text{A}/\text{cm}^2$  and the highest  $i_G$  values are determined at 60 °C (19  $\mu\text{A}/\text{cm}^2$ , approximately). This fact confirms that galvanic current density increases with temperature, since, in general, temperature enhances corrosion rate [22, 28]. At higher temperatures, the passive layer formed on the surface of the material possesses worse corrosion behaviour; consequently, galvanic corrosion rate increases. Wang reported that the porosity of the passive film increases with temperature; in addition the chemical composition and/or physical structure of the passive film changes [37].

As regards galvanic potential presents a general tendency towards more positive values with time, in particular, at 60 °C. Therefore, passivity is expected in polluted  $\text{H}_3\text{PO}_4$  solutions. The galvanic potential values are of the same magnitude order, being for the last hours of the test, more noble at the highest temperature (60 °C).

One of the most remarkable characteristics of uniform corrosion processes is to present low-amplitude potential and current signals [18]. In this sense, Figure 4 shows that the galvanic current density and galvanic potential profiles present very few individual events, especially for the lowest studied temperatures (25 and 40 °C); this is typical in uniform corrosion processes [19].

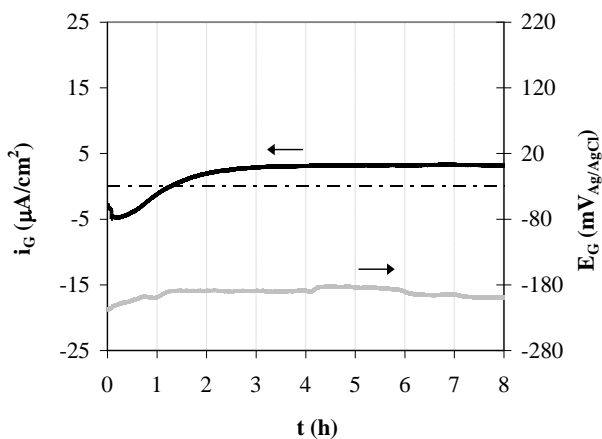
### 3.2.2. Statistical analysis in the time domain

In order to obtain the localisation index (LI), a statistical analysis of signal fluctuation was performed. This index could be useful to discriminate between different corrosion mechanisms and it has been calculated as follows:

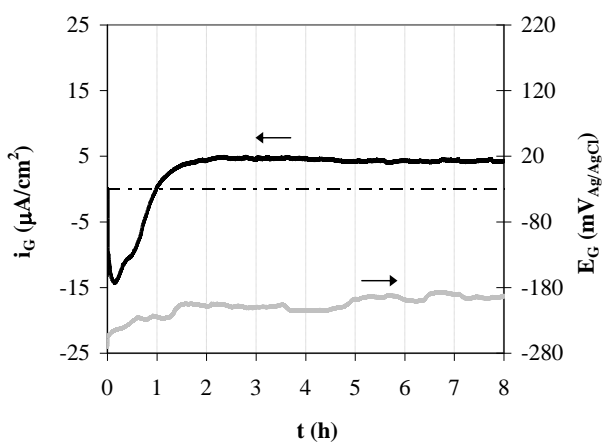
$$\text{LI} = \frac{\sigma_i}{i_{\text{rms}}} \quad (1)$$

where  $\sigma_i$  is the current density standard deviation and  $i_{\text{rms}}$  is the root mean square of the current density; therefore, LI is always between 0 and 1. Several authors indicate that LI values higher than 0.1 are associated with a typical localised corrosion process, while LI values closer to 0 (lesser than 0.05

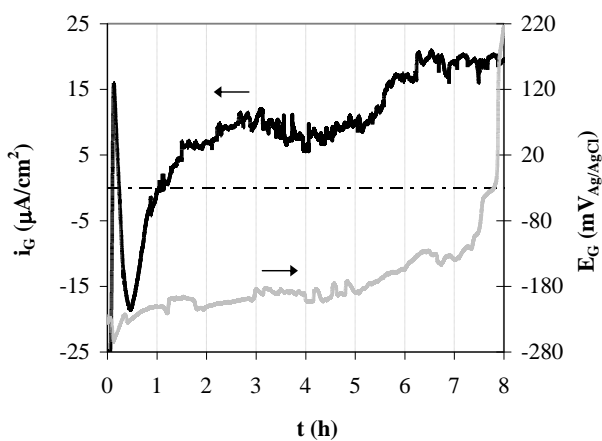




A) Galvanic corrosion profiles at 25 °C



B) Galvanic corrosion profiles at 40 °C



C) Galvanic corrosion profiles at 60 °C

**Figure 4.** Galvanic current density and galvanic potential profiles of the base AISI 316L SS/MPA welded AISI 316L SS pair in polluted H<sub>3</sub>PO<sub>4</sub> solutions at different temperatures.

or 0.01, depending on authors) are associated with a uniform corrosion process [19, 38]. However, Mansfeld [39] suggests that it is doubtful that a single index derived by statistical methods can identify a certain corrosion mechanism because he calculated LI values for uniform corrosion processes and they were greater than 0.1.

Figure 5 shows the LI values of the base AISI 316L SS/MPA welded AISI 316L SS pair calculated for each hour of the tests at the different temperatures analysed. As it can be observed in Figure 5, once the system stabilises, the LI values are close to or under the limit of uniform corrosion processes (during the eighth hour, LI values are lower than 0.05 for all temperatures). When the trend of the experimental data is not significant, the LI values are practically lower than 0.05 at all studied temperatures. It is worth noting that the maximum LI values correspond to the first hours of the tests, probably due to the sharp trend of the experimental data during the first hours. Since LI values are much closer to 0.01 than to 0.1, uniform corrosion process might be expected for the base AISI 316L SS/MPA welded AISI 316L SS galvanic pair in phosphoric acid solutions [19, 38], verifying the results obtained after the examination of the profiles.

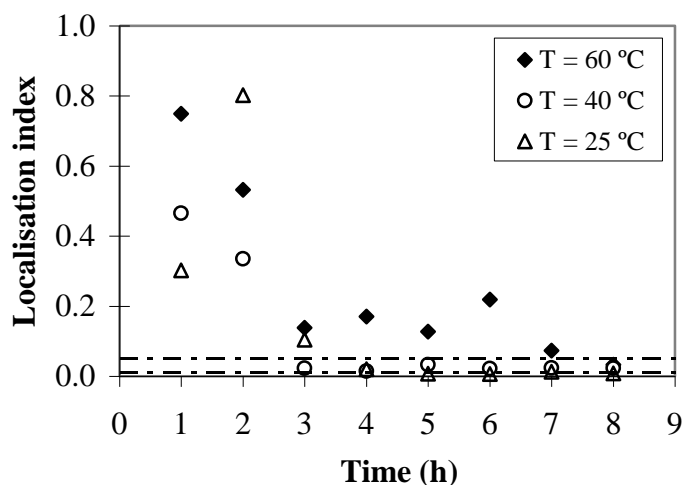


**Figure 5.** Localisation index (LI) values of the base AISI 316L SS/MPA welded AISI 316L SS pair calculated for each hour of the tests at different temperatures.

### 3.2.3. Dependence of the galvanic current density values on temperature in polluted $H_3PO_4$ media according to Arrhenius plot.

In general, temperature increases the rate of most reactions according to Arrhenius equation [40]. In the case of electrochemical reactions, temperature can favour the kinetics of corrosion reactions and, more specifically, the anodic dissolution of the metal [41-43]. The activation energy of the corrosion process can be obtained from Arrhenius-type plots according to the following equation:

$$i_{\text{cor}} = A \cdot \exp\left(-\frac{E_a}{RT}\right) \quad (2)$$

where  $E_a$  is the molar activation energy of the process (J/mol),  $R$  is the universal gas constant (8.314 J/(mol K)),  $T$  is the temperature (K) and  $A$  is a constant. Using the logarithm of the Arrhenius equation, the following expression is obtained:

$$\log(i_{\text{cor}}) = \log(A) - \frac{E_a}{2.303RT} \quad (3)$$

Therefore, the activation energy values of a galvanic corrosion process can be determined from the slope of  $\log(i_G)$  versus  $1/T$  plots [44]. The molar activation energy of an electrochemical process refers to the energy level that must be overcome by one electron in the exchange through the electrode/electrolyte interphase. Moreover, the Arrhenius equation indicates that the greater the dependence of the corrosion rate on temperature, the higher the  $E_a$  values [45].

Figure 6 shows the mean galvanic current density values of the base AISI 316L SS/MPA welded AISI 316L SS pair after system stabilisation (from the third hour of the tests at 25-40 °C and from the seventh hour of the test at 60 °C), plotted according to Equation 3.

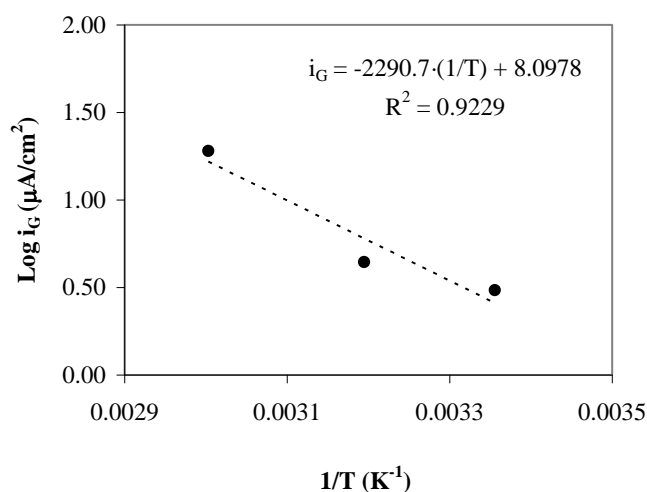


**Figure 6.** Dependence of the mean values of the galvanic current densities, once the registers were stabilised, of the base AISI 316L SS/MPA welded AISI 316L SS pair on the temperature according to Arrhenius plot.

Galvanic current density values increased with temperature according to Arrhenius plot. From the value of the slope shown in Figure 6,  $E_a$  value of the galvanic pair is 43.86 kJ/mol. This is a high energy activation value and of the same magnitude order as those obtained by Benabdellah [46], which indicates a high increase of galvanic current density with temperature in this polluted phosphoric acid media.

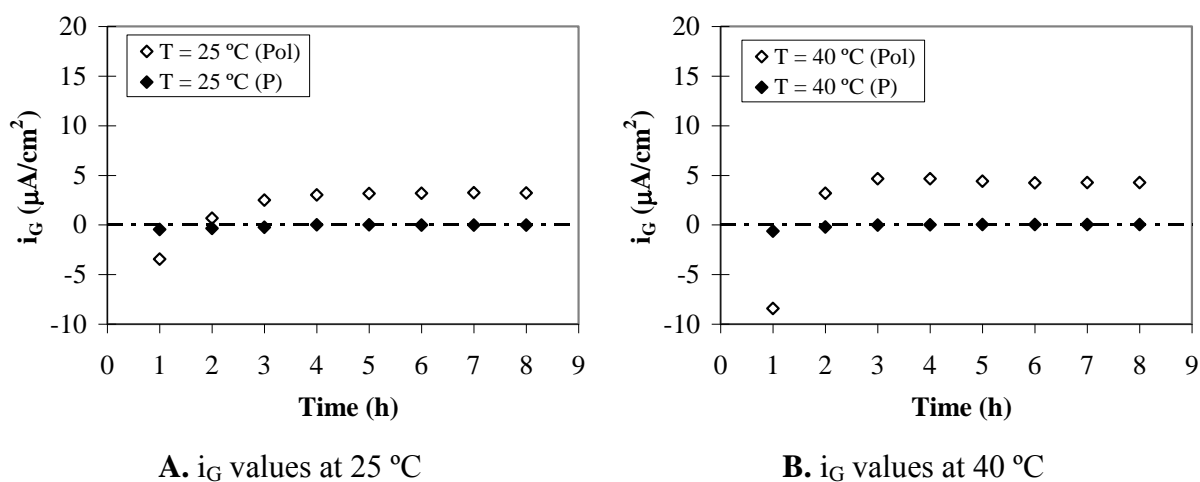
### 3.3. Comparison of the galvanic corrosion in pure and polluted phosphoric acid media

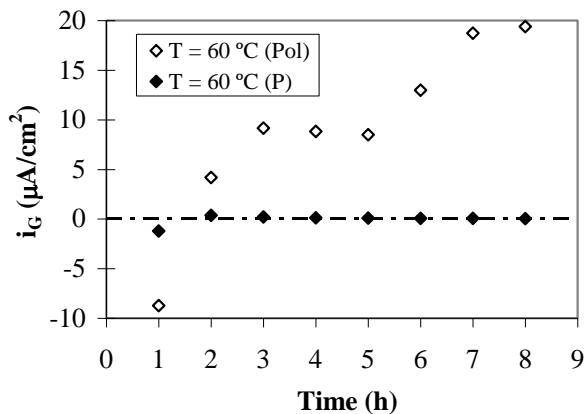
In order to observe the effect of impurities on the galvanic current densities as well as on the galvanic potentials of the base AISI 316L SS/MPA welded AISI 316L SS in phosphoric acid solutions,

results obtained in this work were compared with experiments conducted previously in pure phosphoric acid solutions [47]. The tests were carried out in 40 wt. % phosphoric acid solutions (like those used in this work), but without sulphuric acid and chloride impurities, at 25, 40 and 60 °C and Re of 1456. Figure 7 shows the mean values of the galvanic current density and galvanic potential for the each of the eight hours of the ZRA tests in pure and polluted 40 wt. % phosphoric acid solutions.

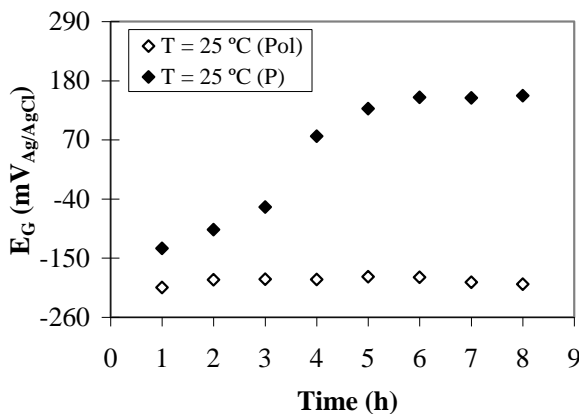
The galvanic current density profiles follow the same trend in pure and polluted H<sub>3</sub>PO<sub>4</sub> solutions. During the first hour of the tests the mean galvanic current densities possess negative values whereas, they shift towards more positive values with time, evidencing the corrosion of the base AISI 316L SS. The mean *i<sub>G</sub>* values during the first hour of the tests are less negative in pure phosphoric acid solutions than in polluted solutions. Subsequently, the *i<sub>G</sub>* values are less positive (very close to zero) than in polluted media, indicating that impurities increase corrosion rate both in the base and the welded AISI 316L SS. On the other hand, galvanic current density values are almost constant in pure phosphoric acid solutions from the second hour until the end of the tests, whereas *i<sub>G</sub>* values in polluted solutions hardly vary from the third hour until the end of the experiments performed at 25 and 40 °C, however, at 60 °C *i<sub>G</sub>* stabilises during the last two hours of the test. In this case, impurities seem to hinder passivation of AISI 316L SS. Similarly, the effect of temperature on *i<sub>G</sub>* is much more significant in polluted than in pure phosphoric acid solutions, since the increase of temperature does not exerted a considerable change on the galvanic current densities in pure solutions; however, temperature modifies *i<sub>G</sub>* values for the alloy in polluted acid media.

As regards the galvanic potentials, they are always more positive working under pure than under polluted phosphoric acid solutions. The general trend of the galvanic potentials in pure H<sub>3</sub>PO<sub>4</sub> media is to increase with time, whereas in polluted solutions, the galvanic potentials shift more slowly towards more positive values. These results confirm that impurities make passivation of the alloy more difficult.

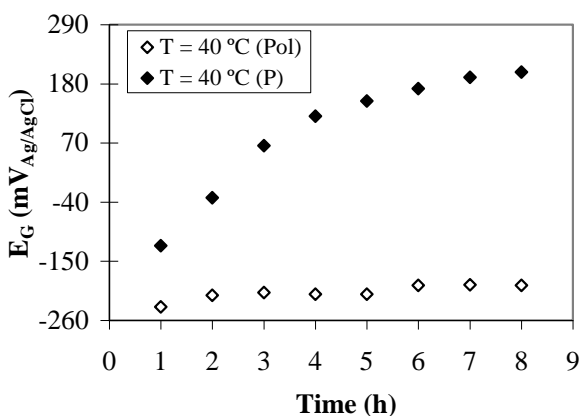




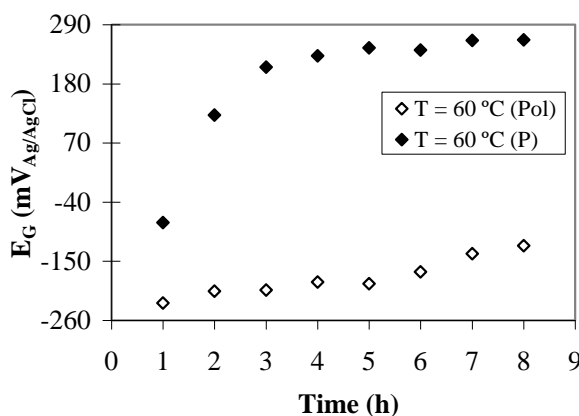
C.  $i_G$  values at 60 °C



D.  $E_G$  values at 25 °C



E.  $E_G$  values at 40 °C



F.  $E_G$  values at 60 °C

**Figure 7.** Mean values of the galvanic current density and galvanic potential of the base AISI 316L SS/MPA welded AISI 316L SS pair in pure and polluted  $H_3PO_4$  solutions at different temperatures. The letters P and Pol means pure and polluted, respectively, referring to the phosphoric acid solution.

#### 4. CONCLUSIONS

In this work, the galvanic corrosion of the base AISI 316L stainless steel /micro-plasma arc welded AISI 316L stainless steel pair in phosphoric acid solutions polluted with sulphuric acid and chlorides was studied using the Zero-Resistance Ammeter technique. The study was performed at different temperatures (25-60 °C) under flowing conditions (Reynolds number of 1456). The main findings obtained from this work are presented below.

1. The micro-plasma arc welding technique modifies the microstructure of the alloy. The base alloy possesses a single austenitic microstructure whereas the welded SS presents three distinct zones, a weld zone with delta-ferrite and columnar grains, a HAZ one with large austenitic grains and the zone, farther from the weld, the base zone, with equiaxed austenitic grain distribution.

2. Galvanic current densities are negative during the first hour of the tests at all temperatures studied indicating that the welded alloy is corroding. Subsequently, the galvanic current densities shift towards positive values (corrosion of the base alloy) and then they stabilise (during the third hour of the tests at 25 and 40 °C and during the last two hours of the test at 60 °C), causing passivation. The highest  $i_G$  values are obtained at 60 °C, indicating that temperature increases galvanic corrosion.

3. Galvanic potential profiles seem to present a general tendency towards more positive values with time, in particular, for the experiments performed at 60 °C. Therefore, passivity is expected.

4. The galvanic current density and galvanic potential profiles present very few individual events and quite low amplitudes, typical in uniform corrosion processes. This fact agrees with localisation index values.

5. Galvanic corrosion increases with temperature according to Arrhenius plot showing a high energy activation that indicates a higher dependence of the galvanic current density with temperature.

6.  $H_2SO_4$  and  $Cl^-$  impurities increase galvanic corrosion rates and hinder passivation compared to pure phosphoric acid solutions.

#### ACKNOWLEDGMENTS

This work was supported by the Spanish MAEC (PCI Mediterráneo C/8196/07, C/018046/08, D/023608/09, D/030177/10). The authors also wish to express their gratitude to Dr. Asunción Jaime for her translation assistance.

#### References

1. J. Mendoza-Canales and J. Marín-Cruz, *Int. J. Electrochem. Sci.*, 3 (2008) 346.
2. A.Y. Musa, A.A.H. Kadhum, A. Bakar-Mohamad, A. Razak-Daud, M. Sobri-Takriff, S. Kartom-Kamarudin and N. Muhamad, *Int. J. Electrochem. Sci.*, 4 (2009) 707.
3. P. Barraco, G. Chiaro and A. Barbera, *Nutr. Cycl. Agroecosyst.*, 26 (1990) 281.
4. L. Narváez, E. Cano and D.M. Bastidas, *J. Appl. Electrochem.*, 35 (2005) 499.
5. A.I. Almarshad and D. Jamal, *J. Appl. Electrochem.*, 34 (2004) 67.
6. A.S. Hamdy, E. El-Shenawy and T. El-Bitar, *Int. J. Electrochem. Sci.*, 1 (2006) 171.
7. J. Oñoro, *Int. J. Pres. Ves. Pip.*, 86 (2009) 656.
8. C. Meola, A. Squillace, F.M.C. Minutolo and R.E. Morace, *J. Mater. Process. Tech.*, 155-156 (2004) 1893.
9. J.F. Lancaster, *Metallurgy of welding*, Woodhead Publishing Limited, Cambridge (1999).
10. S. Lamb, *Stainless steels and nickel alloys*, Casti Publishing Inc., Canada (2002).
11. O. Martín, P. De Tiedra, M. López, M. San-Juan, C. García, F. Martín and Y. Blanco, *Mater. Design*, 30 (2009) 68.
12. D. Özyürek, *Mater. Design*, 29 (2008) 597.
13. F. Karçl, R. Kaçar and S. Gündüz, *J. Mater. Process. Tech.*, 209 (2009) 4011.
14. T. Hemmingsen, H. Hovdan, P. Sanni and N.O. Aagotnes, *Electrochim. Acta*, 47 (2002) 3949.
15. S.A.M. Refaey, F. Taha and A.M. Abd El-Malak, *Int. J. Electrochem. Sci.*, 1 (2006) 80.
16. S.C. Dexter and J.P. LaFontaine, *Corrosion*, 54 (1998) 851.

17. M.G. Pujar, N. Parvathavarthini, R.K. Dayal and H.S. Khatak, *Int. J. Electrochem. Sci.*, 3 (2008) 44.
18. J.R. Kearns, D.A. Eden, M.R. Yaffe, J.V. Fahey, D.L. Reichert and D.C. Silverman, *ASTM Standardization of Electrochemical Noise Measurement*, ASTM STP 1277, Pennsylvania (1996).
19. F.J. Botana, A. Aballe and M. Marcos, *Ruido Electroquímico. Métodos de análisis*, Septem Ediciones, Oviedo (2002).
20. A. Bellaouchou, A. Guenboru and A. Benbachir, *Corrosion*, 49 (1993) 656.
21. S. El Hajjaji, L. Aries, J. Audouard and F. Dabosi, *Corros. Sci.*, 37 (1995) 927.
22. A. Guenbour, H. Iken, N. Kebkab, A. Bellaouchou, R. Boulif and A. Benbachir, *Appl. Surf. Sci.*, 252 (2006) 8710.
23. H. Iken, R. Basseguy, A. Guenbour and A. Ben-Bachir, *Electrochim. Acta*, 52 (2007) 2580.
24. A. Guenbour, M.A. Hajji, El M. Jallouli and A. Ben-Bachir, *Appl. Surf. Sci.*, 253 (2006) 2362.
25. L. Jeffus, *Welding. Principles and Applications*, Delmar Thomson Learning, USA (1997).
26. G.F. Vander Voort, *Metallography. Principles and practice*, ASM International, Ohio (1999).
27. M.T. Montañés, R. Sánchez-Tovar, J. García-Antón and V. Pérez-Herranz, *Int. J. Electrochem. Sci.*, 5 (2010) 1934.
28. P. Becker, *Phosphates and phosphoric acid. Raw materials, technology, and economics of the wet process*, Marcel Dekker, New York (1989).
29. B.M. Patchett and J. Bringas, *The Metals Blue Book. Filler metals.*, CASTI Publishing Inc. and American Welding Society (AWS), Edmonton (1998).
30. I.H. Lo and W.T. Tsai, *Mater. Sci. Eng. A-Struct.*, 355 (2003) 137.
31. M.G. Pujar, R.K. Dayal, T.P.S. Gill and S.N. Malhortra, *J. Mater. Sci. Lett.*, 18 (1999) 823.
32. T.-Y. Kuo and H.-T. Lee, *Mater. Sci. Eng. A-Struct.*, 338 (2002) 202.
33. M. Reffas, R. Sabot, M. Jeannin, C. Berziou and Ph. Refait, *Electrochim. Acta*, 54 (2009) 4389.
34. E. Almeida, D. Pereira, M.O. Figueiredo, V.M.M. Lobo and M. Morcillo, *Corros. Sci.*, 39 (1997) 1561.
35. S.R. Moraes, D. Huerta-Vilca and A.J. Motheo, *Prog. Org. Coat.*, 48 (2003) 28.
36. G.T. Burstein, C. Liu and R.M. Souto, *Biomaterials*, 26 (2005) 245.
37. J.H. Wang, C.C. Su and Z. Szklarskasmialowska, *Corrosion*, 44 (1988) 732.
38. R.A. Cottis and R.S. Turgoose, *Electrochemical Impedance and Noise*, B.C. Syrett, Corrosion Testing Made Easy Series, NACE International, Houston (1999).
39. F. Mansfeld and Z. Sun, *Corrosion*, 55 (1999) 915.
40. A.J. Bard and L.R. Faulkner, *Electrochemical methods. Fundamentals and Applications*, John Wiley & Sons Inc., USA (2001).
41. L.F. Garfias-Mesias and J.M. Sykes, *Corros. Sci.*, 41 (1999) 959.
42. N.J. Laycock, *Corrosion*, 55 (1999) 590.
43. A. Pardo, E. Otero, M.C. Merino, M.D. López, M.V. Utrilla and F. Moreno, *Corrosion*, 56 (2000) 411.
44. M. El Sherif, K.M. Ismail and W.A. Badawy, *Electrochim. Acta*, 49 (2004) 5139.
45. P.W. Atkins, *Physical Chemistry*, Oxford University Press, USA (1998).
46. M. Benabdellah and B. Hammouti, *Appl. Surf. Sci.*, 252 (2005) 1657.
47. R. Sánchez-Tovar, M.T. Montañés, J. García-Antón, A. Guenbour and A. Ben-Bachir, *Corros. Sci.*, 53 (2011) 1237.